Determination of viscosity in shear-induced melting two-dimensional dusty plasmas using Green-Kubo relation

Dong Huang, Shaoyu Lu, and Yan Feng *

Center for Soft Condensed Matter Physics and Interdisciplinary Research, School of Physical Science and Technology, Soochow University, Suzhou 215006, China

(Received 27 September 2020; accepted 5 January 2021; published 25 January 2021)

Langevin dynamical simulations of shear-induced melting two-dimensional (2D) dusty plasmas are performed to study the determination of the shear viscosity of this system. It is found that the viscosity calculated from the Green-Kubo relation, after removing the drift motion, well agrees with the viscosity definition, i.e., the ratio of the shear stress to the shear rate in the sheared region, even the shear rate is magnified ten times higher than that in experiments. The behaviors of shear stress and its autocorrelation function of shear-induced melting 2D dusty plasmas are compared with those of uniform liquids at the same temperatures, leading to the conclusion that the Green-Kubo relation is still applicable to determine the viscosity for shear-induced melting dusty plasmas.

DOI: 10.1103/PhysRevE.103.013211

I. INTRODUCTION

Viscosity, or shear viscosity, η, is an important transport coefficient to characterize the momentum flux in fluids [1–5]. As a typical quantity of a fluid, viscosity is defined as the ratio of the shear stress to the shear rate [1,5]. In experiments, the viscosity can be measured using its definition. For example, in a rheometer [6], the shear stress can be easily applied by a moving boundary, then the liquid inside would flow with a velocity gradient, thus the viscosity can be determined from its definition. The Green-Kubo relation [1–5], derived from the equilibrium statistical mechanics, is often used to measure the transport coefficients like diffusion, viscosity, and thermal conductivity, from the random thermal motion of individual particles of the fluids, without any macroscopic shear stress or shear rate. In [7], the Green-Kubo relation is used in the Lenard-Jones liquid containing flows to determine the shear viscosity. It is found that, in this Lenard-Jones liquid with flows, the determined viscosity from the Green-Kubo relation is roughly close to the viscosity definition when the shear rate is small, however, when the shear rate is larger, the Green-Kubo relation is not accurate any more [7] due to the fact that the distribution of the time-averaged dissipative fluxes deviates from the Gaussian too much, as explained in [7].

Dusty plasma, or complex plasma, refers to a collection of highly charged micron-sized dust particles in the plasma environment [8–17]. In the typical laboratory conditions, these dust particles are charged to $\sim -10^4\, e$, so that they can be suspended in the sheath forming a single layer, i.e., the two-dimensional (2D) dusty plasma [18,19]. These dust particles are strongly coupled, interacting with each other through the Yukawa repulsion [20]. In dusty plasma experiments, the dynamics of individual dust particles can be directly studied at the kinetic level using the diagnostic of the video imaging [8–15]. Various transport procedures are experimentally investigated in dusty plasmas, like diffusion [21], viscosity [22–26], and thermal conductivity [27]. In [23–26,28], by applying two laser beams to generated two counterpropagating flows, the solid lattice of the 2D dusty plasma melts, causing shear-induced melting. While using the Navier-Stokes equation to describe the shear-induced melting (or the shear-induced liquid) dusty plasmas, the viscosity is determined directly from the the profile of the flow velocity [23,25,26]. In [24,29], after the flow is generated in 2D dusty plasmas, the viscosity is determined from its definition of the ratio of the shear stress to the shear rate. For uniformly heated dusty plasma experiments, the Green-Kubo relation is used to determine the viscosity [22,30] whose results are consistent with those from either other methods or simulations at similar conditions [22], although, in principle, the Green-Kubo relation is for the equilibrium state without the friction, not for the steady state of dusty plasmas with the frictional gas drag.

Simulations [31–38] are widely used in the studies of dusty plasmas, especially for the parameter ranges which cannot be easily realized in experiments. The viscosity of 2D dusty plasmas has been quantified in various simulations [31–36]. In [31], the Green-Kubo relation is used with the frictionless MD simulations to determine the viscosity, which agrees with the viscosity determined from the drift velocity profile in shear-induced melting experiments [23]. In [32], two types of simulations (the SLLOD [39] and the introducing momentum methods) are performed, so that the shear viscosity values are obtained and the shear-thinning effect of dusty plasmas is discovered. Although the Green-Kubo relation is strictly valid for the equilibrium state (without the friction), the data from the Langevin simulations of dusty plasmas (including the frictional gas drag) are also used with the Green-Kubo relation [33], and the resulting viscosity seems to be still accurate. However, until now, we have not find any previous study whether the Green-Kubo relation is still applicable in

* fengyan@suda.edu.cn

the shear-induced melting dusty plasmas, as we will try here with the simulation data first.

This paper is organized as follows. In Sec. II, we introduce our newly developed Langevin dynamical simulation method to mimic the shear-induced melting dusty plasma experiments. In Sec. III, we try to use the Green-Kubo relation with our simulated shear-induced melting data to calculate the viscosity, and compare it with the viscosity definition, i.e., the ratio of the shear stress to the shear rate. Furthermore, we also compare the obtained viscosity from the shear-induced melting data with that from the uniform liquid at the same temperature. The underlying statistics of the sheared dusty plasmas are also discussed. Finally, it is our summary that, for the shear-induced melting 2D dusty plasmas, the Green-Kubo relation is still applicable to determine the viscosity, even though the simulated shear rate is increased to ten times higher than the maximum of the experimental value.

II. SIMULATION METHODS

Following the tradition [11,15,40,41], we use two dimensionless parameters to characterize 2D dusty plasmas, which are the screening parameter κ and the coupling parameter Γ. The screening parameter is defined as $\kappa = a/\lambda_D$, where a is the Wigner-Seitz radius [11], and λ_D is the Debye length. The coupling parameter Γ is defined as $\Gamma = Q^2/(4\pi\epsilon_0 a k_B T)$, the ratio of the potential energy between two neighboring particles to the averaged kinetic energy of one particle. Here, T is the kinetic temperature of dust particles and k_B is the Boltzmann constant. The inverse of the nominal 2D dusty plasma frequency [11], $\omega_{pd}^{-1} = (Q^2/2\pi\varepsilon_0 m a^3)^{-1/2}$, is used to normalize the time scale, and the Wigner-Seitz radius a is used to normalize the lengthscale.

We use Langevin dynamical simulations to mimic 2D dusty plasmas. The equation of motion [33,42–44] of our simulated particles is

$$m\ddot{\mathbf{r}}_i = -\nabla\Sigma_j\phi_{ij} - \nu m\dot{\mathbf{r}}_i + \xi_i(t), \tag{1}$$

where the term of $-\nabla\Sigma_j\phi_{ij}$ is the particle-particle interaction, while $\nu m\dot{\mathbf{r}}_i$ is the frictional gas drag. The last term on the right-hand side (RHS) $\xi_i(t)$ is the Langevin random kicks [40]. In our simulations, the interparticle interaction is the Yukawa repulsion [20], $\phi_{ij} = Q^2\exp(-r_{ij}/\lambda_D)/4\pi\epsilon_0 r_{ij}$, where r_{ij} is the distance between the particles i and j.

The main purpose of our simulations is to mimic the shear-induced melting in 2D dusty plasmas, similar to the corresponding experiments [23,28]. In our simulations, we specify the initial conditions of the system in the solid regime, so that the simulated system is in the solid lattice initially, like the experiments found in [23,28]. Then, to mimic the manipulation from two laser beams in these shear-induced melting experiments [23,28], we apply two additional forces on the RHS of Eq. (1), which are $\mathbf{F}_1 = A\exp[-(y-y_0)^2/0.25a^2]ma\omega_{pd}^2\mathbf{x}$ and $\mathbf{F}_2 = -A\exp[-(y+y_0)^2/0.25a^2]ma\omega_{pd}^2\mathbf{x}$ in the $\pm\mathbf{x}$ directions, centered at the locations of $y = \pm y_0$. If these two forces are not too small, two counterpropagating flows would be generated, so that the simulated 2D Yukawa lattice would melt to the liquid state.

Here are some details in our simulations for the shear-induced melting 2D dusty plasmas. In total, we simulate $N = 1024$ dust particles constrained within a rectangular box in the x-y plane, with the dimensions of $61.1a \times 52.9a$, using the periodic boundary conditions. The screening parameter is specified as the constant of $\kappa = 0.5$, while the coupling parameter is initially set as $\Gamma = 1000$, so that these particles would self-organize into a solid lattice at first. Here, we keep the value of y_0 as the constant of $y_0 = 9.4\,a$, while the amplitude of the shear force A is varied from 0.04 to 1.4 in units of $ma\omega_{pd}^2$ to mimic the different levels of the manipulation laser power in experiments. The gas damping rate is chosen as $\nu = 0.03\,\omega_{pd}$, a typical value in experiments [28]. The time step is chosen to be small enough, so that the fastest particle cannot move beyond the distance of $a/2000$ in one step, as in [45]. When the system reaches the steady state after the shear force is applied, the positions and velocities of all particles in the next 4×10^8 steps are recorded for the latter data analysis.

Besides the shear-induced melting simulations described above, we also perform the traditional uniform simulations of 2D Yukawa liquids, as in [33,46]. In these uniform liquid simulations, the equation of motion is just Eq. (1), without any other forces on the RHS. The screening parameter is set as the constant of $\kappa = 0.5$, while the Γ value is specified to various values in the liquid regime, as we will describe later. The gas damping rate is unchanged as $\nu = 0.03\,\omega_{pd}$. Other simulation details are identical with [46].

III. RESULTS AND DISCUSSIONS

A. Shear viscosity of shear-induced melting systems

Two steady sheared flows are generated from our simulated shear-induced melting 2D dusty plasmas, as one example shown in Fig. 1. The profiles of the drift velocity along the flow direction, and the kinetic temperature calculated from the steady state flow data are presented in Fig. 1. To calculate the drift velocity $\overline{V_x}$, as in [25], first we divide the total simulation box into 54 bins (with the width of a) in the y direction. Then, for each bin, we use the cloud-in-cell algorithm to average the x velocity, i.e., the velocity along the flow direction [25,26,28]. In the drift velocity profile of Fig. 1(a), clearly, there are two prominent peaks in the positive and negative directions, corresponding to a pair of counterpropagating flows generated in the simulations. In our data analysis, we mainly focus on the central region of the laminar flow, where the drift velocity is nearly linear, as magnified in Fig. 1(b).

The kinetic temperature of our simulated shear-induced melting 2D dusty plasma can be obtained by removing the drift flow motion, as shown in Fig. 1(b). We calculate the kinetic temperature due to the motion in the x direction using $k_B T_x = \overline{m(v_x - \overline{V_x})^2}$ averaged for all particles within each bin, where $\overline{V_x}$ is the corresponding drift velocity obtained from the combination of the linear fit of $\overline{V_x}$ in Fig. 1(b) and the y location of each particle. However, since there is no drift motion in the y direction, we use $k_B T_y = \overline{m(v_y)^2}$ directly to determine the T_y. Here, the symbol of $\bar{}$ in these equations for T_x and T_y means the cloud-in-cell algorithm averaging, as in the calculation of the drift velocity $\overline{V_x}$. Our obtained kinetic temperature results in Fig. 1(b) show that, in the

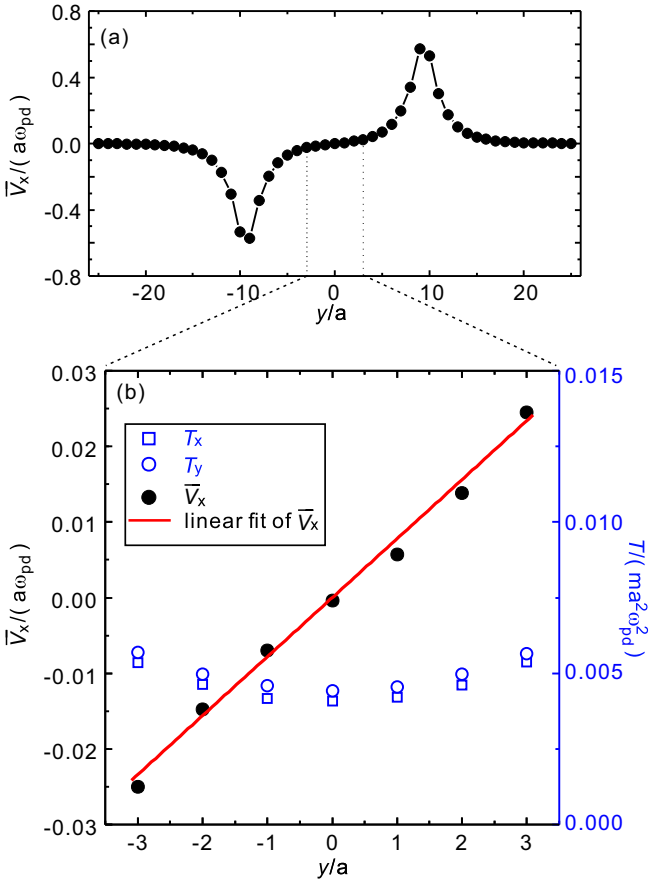

FIG. 1. Profiles of the drift velocity with two counterpropagating flows in (a) our simulated shear-induced melting 2D dusty plasma and (b) the magnified central portion. The kinetic temperatures due to the motions in two directions are also plotted in (b). In the central region, the kinetic temperature does not vary much, while the drift velocity profile is nearly linear, as the linear fit shown in (b). This linear fit can be used to quantify the shear rate there. Here, the obtained shear rate, or the drift velocity gradient, is $\gamma = 0.0078\,\omega_{pd}$, and the corresponding kinetic temperature at the central bin is $T_y = 0.017\,ma^2\omega_{pd}^2$. In our simulations, when we apply different magnitudes of the force, A, the amplitude of the generated counterpropagating flows would be modified, however, the drift velocity profile in the central region of $-3\,a < y < 3\,a$ is always linear. Thus, in our data analysis, we always choose the analyzed region as $-3\,a < y < 3\,a$.

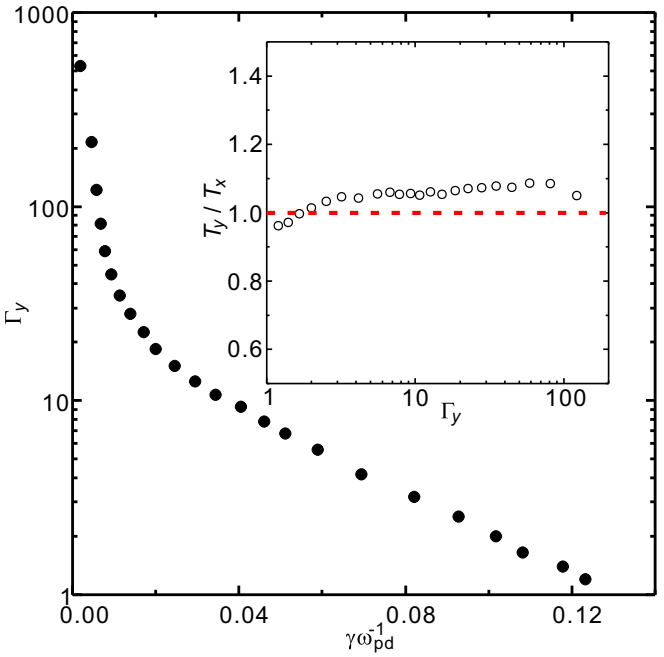

FIG. 2. The coupling parameter Γ_y for the sheared region, as the function of various shear rates. As the shear rate γ increases, the coupling parameter Γ_y decreases monotonically, due to the viscous heating effect [23,28]. The inset show the ratio of the kinetic temperatures due the motions in the two directions, which varies from 0.92 to 1.04. Clearly, for our simulated shear-induced melting dusty plasmas, the anisotropy feature is small, suggesting that the coupling parameter Γ_y can be used to represent the system.

central region, the kinetic temperatures does not spatially vary too much, and this region is nearly isotropic in the kinetic temperatures of T_x and T_y. To simplify the presentation, we will directly use T_y at the central point, and the corresponding Γ_y, to represent the kinetic temperature of the studied central region later. Note, in Fig. 1, the flow velocity and kinetic temperature are both normalized to be dimensionless.

Just like the previous dusty plasma experiments [23], as the shear rate increases, the kinetic temperature of the simulated shear-induced melting dusty plasma increases monotonically, as shown in Fig. 2, although there is a slightly anisotropic feature, as shown in the inset of Fig. 2. In our simulations, when the amplitude of the applied force A increases, the shear rate would be larger, as a result, the kinetic temperature around the central region would be higher, probably due to the viscous heating effect [25,26,28]. Thus, the corresponding coupling parameter Γ_y would reasonably diminish with the shear rate, as shown in Fig. 2. In our simulations, the shear force is applied in the x direction, and the resulting kinetic temperatures due the motions in the two directions might be not exactly the same, i.e., the system contains some anisotropic feature, as shown in Fig. 1(b). In the inset of Fig. 2, we plot the ratio of our obtained T_y to T_x at the central point. Clearly, the ratio of the obtained T_y to T_x varies from 0.92 to around 1.04, i.e., although the anisotropic feature in T_x and T_y exists, but not too much. Thus, it is reasonable to use T_y, and the corresponding Γ_y, to represent the kinetic temperature there. Note it seems that, when the shear rate is larger, the obtained T_y is slightly higher than T_x, probably due to the less collision opportunity in the flow direction, or the x direction.

The time series of the shear stress, or the off-diagonal element of the stress tensor [1,5], in the central melted region from our simulation data are calculated, as two examples shown in Fig. 3. We calculate the shear stress per unit area in the central region using

$$P_{xy} = \frac{1}{A}\sum_{i=1}^{N}\left[m(v_{ix} - \overline{V_{x,i}})v_{iy} - \frac{1}{2}\sum_{j\neq i}^{N}\frac{x_{ij}y_{ij}}{r_{ij}}\frac{\partial\phi(r_{ij})}{\partial r_{ij}}\right], \quad (2)$$

where A is the area of the analyzed central melted region, $\overline{V_{x,i}}$ is the corresponding drift velocity at the location of the particle i, obtained from the linear fit of $\overline{V_x}$ in Fig. 1(b), and

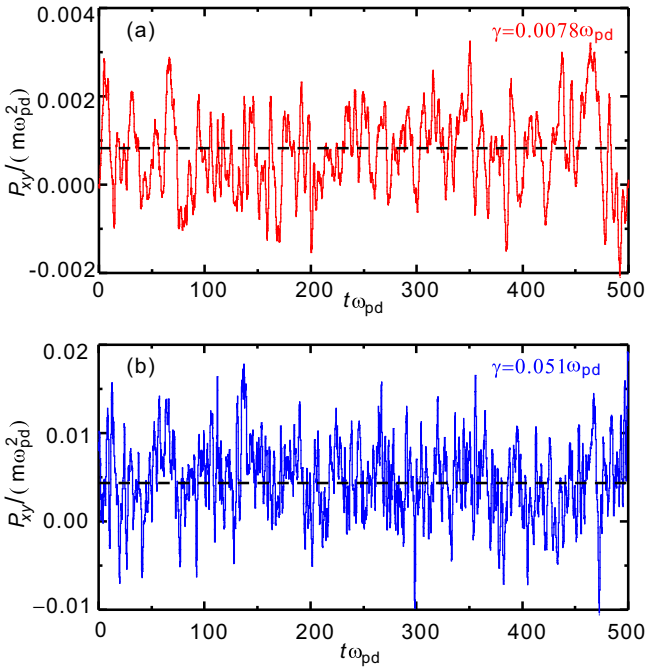

FIG. 3. Time series of the shear stress per unit area P_{xy}, calculated using Eq. (2), from two runs of our shear-induced melting simulations of (a) $\gamma = 0.0078\,\omega_{pd}$ and (b) $\gamma = 0.051\,\omega_{pd}$. Clearly, for shear-induced melting dusty plasmas, when the shear rate γ is higher, the fluctuation of P_{xy} would be more severe, and the averaged value of P_{xy}, as the dashed line shown, would also be larger.

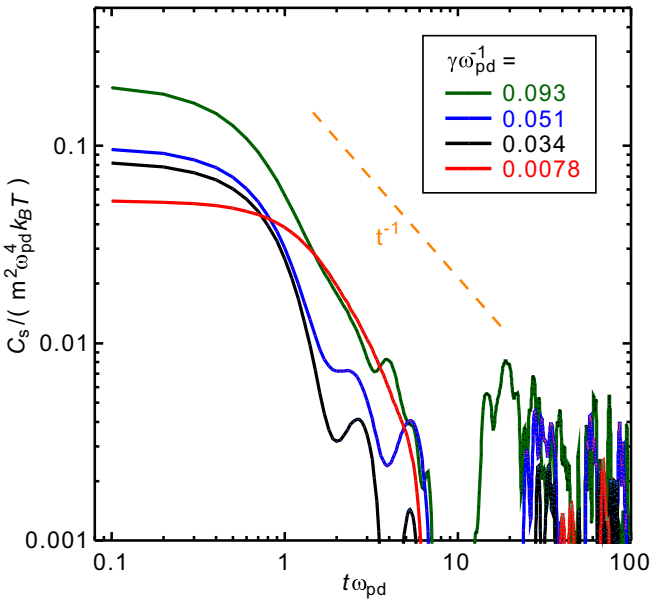

FIG. 4. Shear stress autocorrelation function C_s/T_y, calculated using Eq. (3), from our shear-induced melting simulations, for four different shear rates of $\gamma = 0.0078\,\omega_{pd}$, $\gamma = 0.034\,\omega_{pd}$, $\gamma = 0.051\,\omega_{pd}$, and $\gamma = 0.093\,\omega_{pd}$. These obtained C_s/T_y results are used in Eq. (4) to calculate the viscosity later. Note our obtained C_s/T_y decays faster than t^{-1}, indicating that the long-time tail problem does not exist here [47].

the y coordinate of the particle i. Here, we follow the tradition in [1] to remove the drift velocity while calculating the shear stress per unit area P_{xy} for the systems containing flows. In our simulations, this central melted region refers to $-3a \leqslant y \leqslant 3a$ in the simulation box, containing about 117 particles, where the flow velocity profile is nearly linear as shown in Fig. 1(b). Two panels of Fig. 3 correspond to the time series of shear stress for two values of the shear rate $\gamma = 0.0078\,\omega_{pd}$ and $0.051\,\omega_{pd}$, respectively. From Fig. 3, it seems that, when the shear rate increases, the fluctuation level and the averaged value (dashed lines) of the shear stress would both increase, probably due to the increase of the kinetic temperature in the melted region.

The autocorrelation function of the shear stress fluctuation $C_s(t)$ can be obtained, as examples shown in Fig. 4. Here, we use

$$C_s(t) = \langle [P_{xy}(t) - \overline{P_{xy}(t)}][P_{xy}(0) - \overline{P_{xy}(t)}] \rangle \tag{3}$$

to calculate this autocorrelation function of the shear stress fluctuation. Clearly, the averaged value of the shear stress is removed while calculating since only the fluctuation information is needed in the Green-Kubo relation [7]. In Fig. 4, a few C_s/T_y results corresponding to different shear rates are plotted. Here, we verify that, the decay of C_s/T_y is much faster than $1/t$, i.e., the long-time tail problem does not exist in our simulations here [47].

Using our simulation data, in the central melted region, the shear viscosity determined from the Green-Kubo relation is

$$\eta = \frac{A}{k_B T} \int_0^\infty C_s(t) dt. \tag{4}$$

While using our simulation data, we follow the tradition [22,48] to replace the upper limit of the integration from infinity to the time when $C_s(t)$ crosses zero for the first time. For comparison, we also use the viscosity definition [1–5]

$$\eta = \frac{\overline{P_{xy}(t)}}{\gamma} \tag{5}$$

to determine the value of viscosity. In Fig. 5, the viscosity values calculated from these two methods, Eqs.(4) and (5), are plotted together. Clearly, the results from two methods agree with each other very well since all data points in Fig. 5 overlap with each other. As the coupling parameter Γ_y increases from around 1, the viscosity diminishes first, and then increases. For both of the methods here, the viscosity would have a minimum when the coupling parameter Γ_y is around 15, well consistent with the previous uniform simulations [31,49]. For the typical shear-induced melting dusty plasma experiments [23,28], the shear rate is not very big, at most about $0.0078\omega_{pd}$ in [28] or $0.012\omega_{pd}$ in [23], thus the maximum shear rate in our simulations is about ten times higher. Note that, like the previous shear-induced melting experiments [23,28], the temperature and shear rate are not independent in Figs. 5(a) and 5(b).

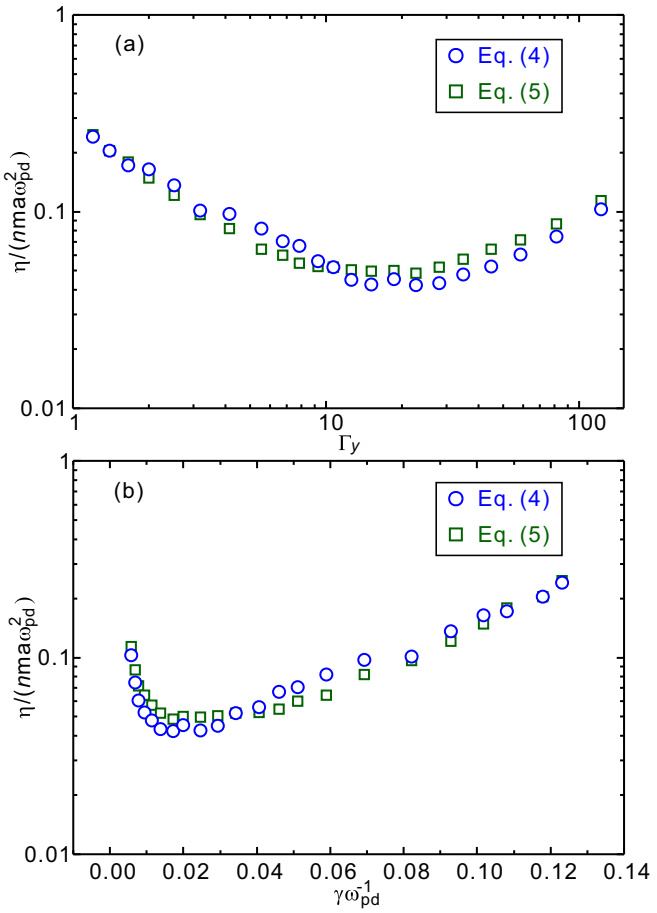

FIG. 5. The obtained viscosity of our simulated shear-induced melting 2D dusty plasmas using two different methods of Eqs. (4) and (5), as the function of (a) the coupling parameters and (b) the shear rate. Clearly, the viscosity values calculated from these two methods agree with each other, since the obtained data points overlap with each other. Note that, for our simulated shear-induced melting dusty plasmas, the coupling parameter Γ and the shear rate γ are not independent, like the previous experiments [23].

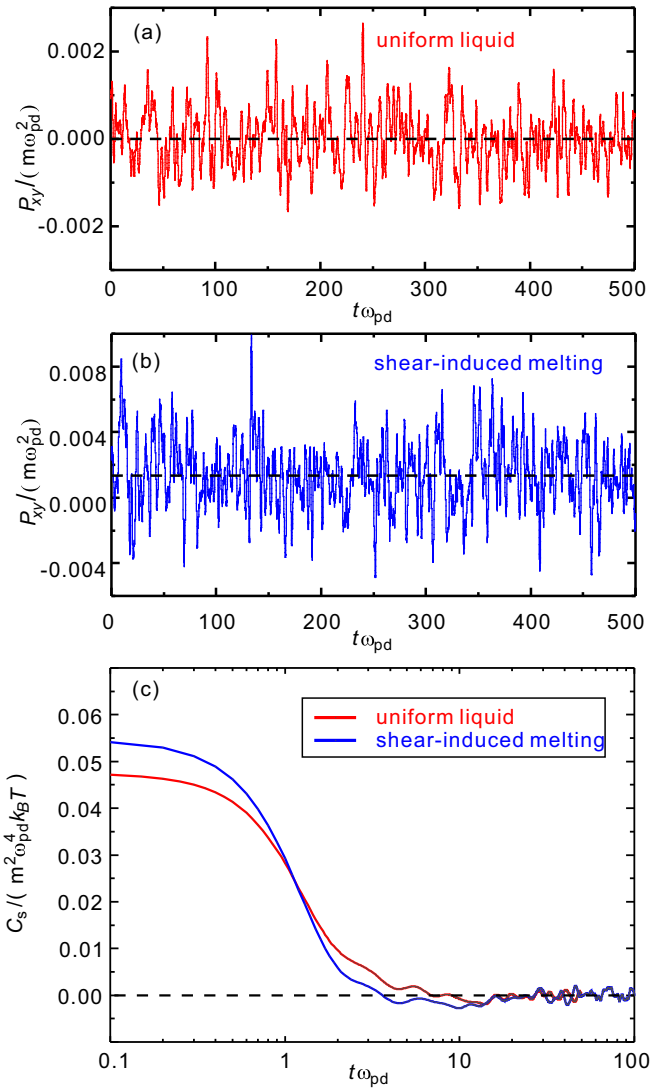

FIG. 6. Time series of the (a,b) shear stress per unit area P_{xy} and (c) the corresponding autocorrelation function C_s/T_y for the uniform liquid and the shear-induced melting system, for the same coupling parameter of $\Gamma_y = 35$. The results show that the fluctuation of P_{xy} in the shear-induced melting system is larger, however, the corresponding C_s/T_y decays much faster.

B. Comparison with viscosity of uniform liquids

For comparison, we also calculate the shear stress per unit area P_{xy} of the simulated uniform liquid at the similar temperature as the shear-induced melting system, as shown in Figs. 6(a) and 6(b). Although the values of the coupling parameter Γ_y of these two runs are nearly the same of about 35, the fluctuation level of P_{xy} for the uniform liquid of Fig. 6(a) is substantially smaller than that for the shear-induced melting system of Fig. 6(b). Furthermore, from Fig. 6, the averaged value of P_{xy} for the shear-induced melting system of Fig. 6(b) clearly deviates from zero, while this averaged value for the uniform liquid is just zero, as often seen from the previous studies [22,31]. For the uniform liquid, the fluctuation of the shear stress comes from the random thermal motion itself, or the temperature of the system. However, for the shear-induced melting system, the overall flow would also further contribute to the fluctuation of P_{xy}, and this overall flow also cause the nonzero averaged value of P_{xy}.

To quantify the shear viscosity using the Green-Kubo relation, we calculate the autocorrelation function of the shear stress C_s for the comparison of the two types of simulations, as shown in Fig. 6(c). Note, here the nonzero averaged value of P_{xy} for the shear-induced melting system is removed while calculating C_s using Eq. (3). Clearly, due to the higher fluctuation level of P_{xy} for the shear-induced melting system, the corresponding C_s has a larger initial value. Of course, for the uniform liquid, the initial value of C_s is smaller. The decay rate of the shear stress autocorrelation function for these two types of systems are different. As seen in Fig. 6(c), the decay of C_s for the shear-induced melting system is clearly quicker than that for the uniform liquid, probably due to the nonzero overall flow in the shear-induced melting system. The autocorrelation function C_s describes the memory effect of the stress, so that

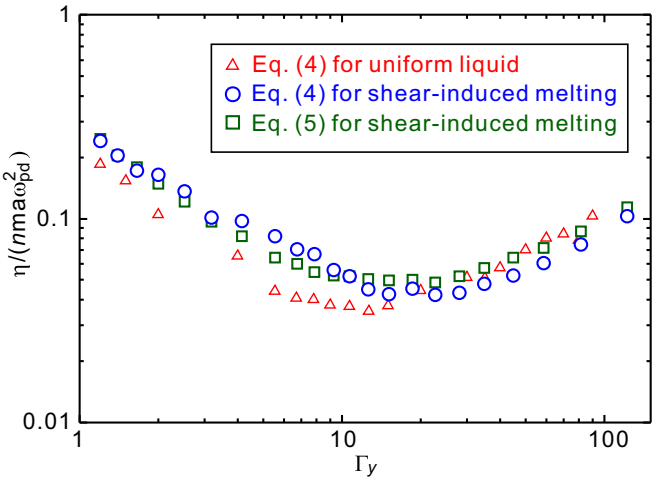

FIG. 7. The viscosity values calculated from our simulated shear-induced melting and uniform liquid data, as the functions of the coupling parameter. Clearly, these obtained viscosity values from these two simulated systems are consistent with each other.

this effect would be reasonably more shortened by the overall flow in the shear-induced melting system.

Our determined results of the shear viscosity from the shear-induced melting and the uniform liquid data are presented in Fig. 7. Clearly, from Fig. 7, the obtained viscosity values from these two simulated systems are consistent with each other. Besides the overall consistency, we can still observe a clear and systematic trend that the obtained viscosity of the uniform liquid data is always lower than that of the shear-induced melting system for the weaker coupling parameter, i.e., $\Gamma_y < 20$, however, for the stronger coupling parameter of $\Gamma_y > 20$, this trend seems to be reversed. Here we would like to mention that our simulated two systems are not the same: the simulated uniform liquid is isotropic, while the shear-induced melting system has a slightly anisotropic feature, as we quantify in the inset of Fig. 2. Following the method in [25,26], we also convert the individual particle data to continuum data using the spatial average of the particle data within those 54 rectangular bins, as described above. From the calculated particle number density profiles, as presented in [50], we find that the number density around the stronger sheared region is much smaller. The density gradient of particle would definitely induce an additional steady momentum transport, similar to the gas viscosity mechanism [51]. Thus, for the higher particle density gradient of the stronger sheared system, the momentum transport is enhanced and the obtained viscosity should be higher. On the other hand, for the typical liquid dusty plasmas, the shear thinning effect has already been discovered [32], which means that the viscosity diminishes when the shear rate increases. Our explanation about the systematic variation trend in Fig. 7 is probably the competition of these two mechanisms, the shear-thinning effect and the number-density gradient induced momentum transport. When the shear is lower, the number density gradient is tiny, the shear thinning effect dominates, so that the viscosity of the shear-induced melting system is smaller, for the data points of $\Gamma_y > 20$ in Fig. 7. However, when the shear is stronger, the temperature of the system is higher, and the number density gradient is also higher as presented in [50], leading to the stronger number-density gradient induced momentum transport [51], thus the obtained viscosity value is higher, for the data points of $\Gamma_y < 20$ in Fig. 7.

From all above, we conclude that, for the shear-induced melting 2D dusty plasmas, the Green-Kubo relation is still applicable to quantify the shear viscosity, and the quantified viscosity well agrees with the viscosity definition of Eq. (5). While calculating the shear stress of the shear-induced melting 2D dusty plasmas, the drift motion should be removed, as in Eq. (2). We also find that, these viscosity values from the shear-induced melting dusty plasmas are consistent with the viscosity of the uniform liquids at the same temperatures.

IV. SUMMARY

We perform Langevin dynamical simulations of shear-induced melting 2D dusty plasmas to study the shear viscosity. We find that the Green-Kubo relation is still applicable to determine the shear viscosity for the shear-induced melting dusty plasmas, and the determined viscosity using this method well agrees with the value obtained from the viscosity definition, i.e., the ratio of the shear stress to the shear rate. In our simulations, we magnify the shear rate about ten times higher than the maximum of the experimental value [23,28], and the determined viscosity results from the Green-Kubo relation still well agree with those from the viscosity definition. To further verify our finding, we also compare the obtained viscosity values of the shear-induced melting dusty plasmas with those of the uniform liquids at the same temperatures. Our simulation results show that the viscosity from these two simulated systems are consistent with each other.

Our developed method of using the Green-Kubo relation with the shear-induced melting dusty plasmas, after removing the drift motion, provides a different approach to determine the shear viscosity. Especially for the higher sheared flows when the drift velocity profile is not linear, in which the viscosity definition cannot be directly used, this modified Green-Kubo relation method is more useful. In addition to this methodology, our findings here also provide understandings of the underlying statistics of the studied system. For the shear-induced melting dusty plasmas, it seems that the fluctuation of the shear stress still can be used to determine the shear viscosity, although the corresponding fluctuation behaviors are modified by the drift motion.

ACKNOWLEDGMENTS

Work was supported by the National Natural Science Foundation of China under Grant No. 11875199, the 1000 Youth Talents Plan, startup funds from Soochow University, and the Priority Academic Program Development (PAPD) of Jiangsu Higher Education Institutions.

[1] D. J. Evans and G. P. Morris, *Statistical Mechanics of Non-equilibrium Liquids*, 2nd ed., (Cambridge University Press, Cambridge, England, 2008).

[2] O. Penrose, *Foundations of Statistical Mechanics* (Pergamon, Oxford, 1970).

[3] P. Perrot, *A to Z of Thermodynamics* (Oxford University Press, Oxford, 1998).

[4] A. L. Fetter and J. D. Walecka, *Theoretical Mechanics of Particles and Continua* (Dover, Mineola, NY, 2003).

[5] J. P. Hansen and I. R. McDonald, *The Theory of Simple Liquids*, 2nd ed. (Elsevier, Amsterdam, 1986).

[6] R. Pal, J. Colloid Interface Sci. **225**, 359 (2000).

[7] D. J. Searles and D. J. Evans, J. Chem. Phys. **112**, 9727 (2000).

[8] H. M. Thomas and G. E. Morfill, Nature (London) **379**, 806 (1996).

[9] L. I, W. T. Juan, C. H. Chiang, and J. H. Chu, Science **272**, 1626 (1996).

[10] R. L. Merlino and J. A. Goree, Phys. Today **57**(7), 32 (2004).

[11] G. J. Kalman, P. Hartmann, Z. Donkó, and M. Rosenberg, Phys. Rev. Lett. **92**, 065001 (2004).

[12] V. E. Fortov, A. V. Ivlev, S. A. Khrapak, A. G. Khrapak, and G. E. Morfill, Phys. Rep. **421**, 1 (2005).

[13] G. E. Morfill and A. V. Ivlev, Rev. Mod. Phys. **81**, 1353 (2009).

[14] A. Piel, *Plasma Physics* (Springer, Heidelberg, 2010).

[15] M. Bonitz, C. Henning, and D. Block, Rep. Prog. Phys. **73**, 066501 (2010).

[16] A. Melzer, A. Schella, J. Schablinski, D. Block, and A. Piel, Phys. Rev. E **87**, 033107 (2013).

[17] E. Thomas, Jr., U. Konopka, R. Merlino, and M. Rosenberg, Phys. Plasmas **23**, 055701 (2016).

[18] Y. Feng, J. Goree, and B. Liu, Phys. Rev. Lett. **100**, 205007 (2008).

[19] K. Qiao, J. Kong, J. Carmona-Reyes, L. S. Matthews, and T. W. Hyde, Phys. Rev. E **90**, 033109 (2014).

[20] U. Konopka, G. E. Morfill, and L. Ratke, Phys. Rev. Lett. **84**, 891 (2000).

[21] B. Liu and J. Goree, Phys. Rev. Lett. **100**, 055003 (2008).

[22] Y. Feng, J. Goree, B. Liu, and E. G. D. Cohen, Phys. Rev. E **84**, 046412 (2011).

[23] V. Nosenko and J. Goree, Phys. Rev. Lett. **93**, 155004 (2004).

[24] P. Hartmann, M. C. Sándor, A. Kovács, and Z. Donkó, Phys. Rev. E **84**, 016404 (2011).

[25] Y. Feng, J. Goree, and B. Liu, Phys. Rev. Lett. **109**, 185002 (2012).

[26] Y. Feng, J. Goree, and B. Liu, Phys. Rev. E **86**, 056403 (2012).

[27] V. Nosenko, S. Zhdanov, A. V. Ivlev, G. Morfill, J. Goree, and A. Piel, Phys. Rev. Lett. **100**, 025003 (2008).

[28] Y. Feng, J. Goree, and B. Liu, Phys. Rev. Lett. **104**, 165003 (2010).

[29] Z. Haralson and J. Goree, Phys. Plasmas **23**, 093703 (2016).

[30] Z. Haralson and J. Goree, Phys. Rev. Lett. **118**, 195001 (2017).

[31] B. Liu and J. Goree, Phys. Rev. Lett. **94**, 185002 (2005).

[32] Z. Donkó, J. Goree, P. Hartmann, and K. Kutasi, Phys. Rev. Lett. **96**, 145003 (2006).

[33] Y. Feng, J. Goree, and B. Liu, Phys. Plasmas **18**, 057301 (2011).

[34] A. Shahzad and M.-G. He, Phys. Scr. **86**, 015502 (2012).

[35] A. Shahzad, A. Aslam, and M.-G. He, Radiat. Eff. Defect Solids **169**, 931 (2014).

[36] S. Landmann, H. Kahlert, H. Thomsen, and M. Bonitz, Phys. Plasmas **22**, 093703 (2015).

[37] Z. Donkó, P. Hartmann, and J. Goree, Mod. Phys. Lett. B **21**, 1357 (2007).

[38] K. Y. Sanbonmatsu and M. S. Murillo, Phys. Rev. Lett. **86**, 1215 (2001).

[39] D. J. Evans and O. P. Morriss, Comput. Phys. Rep. **1**, 297 (1984).

[40] Y. Feng, B. Liu, and J. Goree, Phys. Rev. E **78**, 026415 (2008).

[41] P. Hartmann, A. Z. Kovács, A. M. Douglass, J. C. Reyes, L. S. Matthews, and T. W. Hyde, Phys. Rev. Lett. **113**, 025002 (2014).

[42] Z. Donkó, J. Goree, and P. Hartmann, Phys. Rev. E **81**, 056404 (2010).

[43] Z. Donkó, G. J. Kalman, and P. Hartmann, J. Phys.: Condens. Matter. **20**, 413101 (2008).

[44] L.-J. Hou, A. Piel, and P. K. Shukla, Phys. Rev. Lett. **102**, 085002 (2009).

[45] W. Lin, M. S. Murillo, and Y. Feng, Phys. Rev. E **100**, 043203 (2019).

[46] K. Wang, D. Huang, and Y. Feng, J. Phys. D: Appl. Phys. **51**, 245201 (2018).

[47] Z. Donkó, J. Goree, P. Hartmann, and B. Liu, Phys. Rev. E **79**, 026401 (2009).

[48] Y. Feng, W. Lin, and M. S. Murillo, Phys. Rev. E **96**, 053208 (2017).

[49] G. Faussurier and M. S. Murillo, Phys. Rev. E **67**, 046404 (2003).

[50] See Supplemental Material at http://link.aps.org/supplemental/10.1103/PhysRevE.103.013211 for a description of the number density profiles of the shear-induced melting 2D dusty plasmas with the different levels of the shear rate.

[51] R. B. Bird, W. E. Stewart, and E. N. Lightfoot, *Transport Phenomena* (John Wiley & Sons, New York, 2002).